

Anisotropy-Induced Quantum Interference Between Orthogonal Quantum Dot Exciton States in Semiconductor Cavity Systems

Stephen Hughes¹ and Girish Agarwal^{2,3}

¹*Department of Physics, Queen's University, Kingston, Ontario, Canada, K7L 3N6*

²*Institute for Quantum Science and Engineering and Department of Biological and Agricultural Engineering, Texas A&M University, College Station, Texas 77845*

³*Department of Physics, Oklahoma State University, Stillwater, OK 74078, USA*

(Dated: November 27, 2018)

We describe how quantum dot semiconductor cavity systems can be engineered to exploit anisotropy-induced dipole-dipole coupling between orthogonal dipole states in a single quantum dot. Quantum dots in single-mode cavity structures with spin exciton states, as well as photonic crystal waveguides coupled to spin states or linearly polarized excitons are considered, where the latter can be coupled to chiral points in the Bloch mode. We demonstrate pronounced, almost perfect, dipole-dipole coupling and dipole entanglement effects and study the quantum dynamics of both field-free entanglement evolution and coherently pumped entanglement regimes. In a Mollow triplet regime, where one of the dipoles is pumped, we also explore the incoherent spectra emitted from the orthogonal dipoles and show how the non-pumped dipole can take on the form of a spectral singlet or triplet.

PACS numbers: 42.55.Sa 42.55.Ah 42.50.Lc

Introduction. The ability to manipulate and control spontaneous emission (SE) decay and coherent coupling between quantum dipoles is a key requirement for many applications in quantum optics, including the creation of entangled photon sources and qubit entanglers. Quantum dots (QDs) are especially preferable for studying quantum optical effects due to the large transition dipole moments. A major problem with entangling quantum dots (QDs) is due to their large inhomogeneous broadening, leading to negligible or very small photon-coupling rates for spatially separated QDs. In 2000, Agarwal [1] showed how vacuum-induced interference effects from an anisotropic vacuum can lead to quantum interference effects among decay channels of closely lying states at the same spatial point, even though the dipoles are orthogonal—a phenomenon termed: “anisotropic vacuum-induced interference” (AVI). Subsequently, there have been several related theoretical works, though no reported experiments to our knowledge. Li *et al.* [2] demonstrated AVI using a 3-level atom in a multilayered dielectric medium. Recently, Jha *et al.* [3] studied a QD coupled to a metamaterial surface to predict AVI using nanoantenna designs, which has the potential advantage of remote distance control; the AVI was shown to allow a maximum population transfer between the orthogonal dipoles of around 1%, and similar proposals have been later reported by Sun and Jiang [4]. While interesting, these studies are difficult to realize experimentally, and the predicted population transfer coupling effects are rather weak. Moreover, the plasmonic systems introduce material losses, and large Purcell factor regimes would be necessary to compensate realistic non-radiative decay rates in real QD systems. Metamaterial systems also have very low quantum efficiencies in general [5].

In practical semiconductor QD systems, large radiative

decay rates are necessary and easily achieved in single mode cavity systems. For efficient single photon β factors, slow-light PC waveguides have been shown to yield almost perfect single photons on-chip [6]; these waveguides also exhibit a rich polarization dependence with position, and one can find points of linear polarization or circular polarization. Charge neutral QD excitons in general exhibit either linear polarization or circular polarization if the fine structure splitting (FSS) is negligible (e.g., [7–9]), which indeed can now be controlled with great precision [10]. Charged QD excitons can also be used to study interactions between single spins and photons [11], which is important for quantum networks and distributed quantum computation. It would thus be highly desirable to study and exploit AVI effects in such geometries, using realistic QD exciton states that can be either linearly polarized or spin polarized (charged excitons). Moreover, one would like to go beyond the free-field case of vacuum dynamics and study, e.g., field driven coupling via a pump field where such effects can be more easily accessed experimentally.

In this Letter, we introduce several practical QD photonic systems that can enable pronounced AVI, causing long lived entangled photon states with an almost perfect means of achieving population transfer—a feat that is not possible with spatially separated QD dipoles. Figure 1 shows a schematic of QD exciton states and example photonic systems including a microcavity with a linearly-polarized cavity mode, and a photonic crystal (PC) waveguide that exhibits linear or circular polarization on the so-called L lines (or X points) and C points, respectively [12, 13]. Such systems provide a high degree of anisotropy needed for observing AVI using QDs. Our significant findings are: (i) AVI produces long lived entangled QD states with a population transfer which is

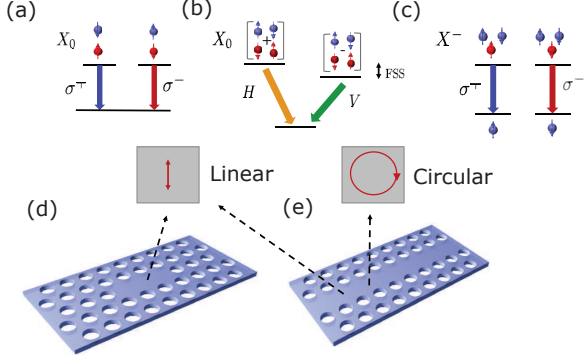


FIG. 1: Example QD states using neutral (a-b) and charged exciton states (c) that can be coupled to L points or C points in a photonic system. The dipole directions are in the plane, caused by stronger quantum confinement in the vertical direction, and the neutral dot excitons may also be split by a small fine structure splitting (FSS). The former L-point coupling can be realized in a microcavity (d) or PC waveguide (e) while the latter C-point can be realized in a PC waveguide.

orders of magnitude larger than in other systems, (ii) selective pumping of the transitions enables one to study features of Mollow triplets which are strictly due to AVI, and (iii) AVI induced coherent coupling of dipoles, where one excited dipole acts as the pump for the other dipole.

Theory. Photon transfer can be rigorously modelled through the the electric-field Green function, which describes the field response at \mathbf{r} to a point source at \mathbf{r}' is defined through $[\nabla \times \nabla \times - \frac{\omega^2}{c^2} \epsilon(\mathbf{r})] \mathbf{G}(\mathbf{r}, \mathbf{r}', \omega) = \frac{\omega^2}{c^2} \mathbf{1} \delta(\mathbf{r} - \mathbf{r}')$, where $\mathbf{G}_{i,j}$ is a second rank tensor and $\mathbf{1}$ is the unit dyad; element $[i, j]$ corresponds to the response in direction i at \mathbf{r} from the j th component of the source at \mathbf{r}' . Planar PC waveguide modes below the light line ($\omega = c|\mathbf{k}|$) will propagate without loss through an ideal structure (neglecting imperfections) and can be written as $\mathbf{f}_{k\omega}(\mathbf{r}) = \sqrt{\frac{a}{L}} \mathbf{e}_{k\omega}(\mathbf{r}) e^{ik_{\omega}x}$, where $\mathbf{e}_{k\omega}(\mathbf{r})$ is the Bloch mode, sharing the same periodicity as the lattice, a is the pitch of the PC, and L is the length of the structure; $\mathbf{e}_{k\omega}(\mathbf{r})$ is normalized from $\int_{V_c} \epsilon(\mathbf{r}) \mathbf{e}_{k\omega}(\mathbf{r}) \cdot \mathbf{e}_{k'\omega'}^*(\mathbf{r}) = \delta_{k\omega, k'\omega'}$, where V_c is the spatial volume of a PC unit-cell. These normalized Bloch modes can be used to obtain the waveguide Green function analytically [14, 15],

$$\mathbf{G}_{\text{wg}}(\mathbf{r}, \mathbf{r}'; \omega) = \frac{ia\omega}{2v_g} \left[\Theta(x - x') \mathbf{e}_{k\omega}(\mathbf{r}) \mathbf{e}_{k'\omega'}^*(\mathbf{r}') e^{ik_{\omega}(x-x')} + \Theta(x' - x) \mathbf{e}_{k'\omega'}^*(\mathbf{r}) \mathbf{e}_{k\omega}(\mathbf{r}') e^{ik_{\omega}(x'-x)} \right], \quad (1)$$

where the terms preceded by Heaviside functions correspond to forward and backwards propagating modes, respectively, and v_g is the group velocity at the frequency on interest. To account for coupling to other modes, one can simply add other contributions to the total Green function: $\mathbf{G}_{\text{tot}} \equiv \mathbf{G} = \mathbf{G}_{\text{wg}} + \mathbf{G}_{\text{o}}$, where the former (dominant) contribution will account for coupling to the

waveguide mode of interest below the light line, while the latter will account for out of plane decay. For a single mode microcavity system, with resonant frequency ω_c and mode profile, $\mathbf{f}_c(\mathbf{r})$, The Green function

$$\mathbf{G}_c(\mathbf{r}, \mathbf{r}'; \omega) \approx \frac{\omega^2 \mathbf{f}_c(\mathbf{r}) \mathbf{f}_c^*(\mathbf{r}')}{\omega^2 - \omega_c^2 - i\omega\Gamma_c}, \quad (2)$$

where at a field antinode the modes can be normalized through $|\mathbf{f}_c(\mathbf{r}_0)|^2 = 1/V_{\text{eff}}\epsilon_b$, with ϵ_b the background effective index. To account for deviations from the mode antinode position and polarization, one can simply define $|\mathbf{f}_c(\mathbf{r})|^2 = \eta(\mathbf{r})/V_{\text{eff}}\epsilon_b$.

Working in a rotating frame with respect to a laser frequency ω_L , we first derive the quantum master equation for the system of QDs interacting with a general photonic reservoir. In the weak-coupling regime, with the system-reservoir coupling given by the dipole interaction in the rotating-wave approximation, we apply the second-order Born and Markov approximations to the interaction Hamiltonian, trace out the electromagnetic degrees of freedom, and after some algebra arrive at the master equation for the reduced density operator [16–18]:

$$\begin{aligned} \dot{\rho} = & -i \sum_n \Delta\omega_n [\sigma_n^+ \sigma_n^-, \rho] - i \sum_{n,n'}^{\substack{n \neq n' \\ n, n'}} \delta_{n,n'} [\sigma_n^+ \sigma_{n'}^-, \rho] \\ & + \sum_{n,n'} \Gamma_{n,n'} \left(\sigma_{n'}^- \rho \sigma_n^+ - \frac{1}{2} \{ \sigma_n^+ \sigma_{n'}^-, \rho \} \right) - \frac{i}{\hbar} [H_{\text{drive}}, \rho], \end{aligned} \quad (3)$$

where $n = a, b; n' = a, b$ for two excitons, $\Delta\omega_n = (\omega'_n - \omega_L)$, $\omega'_n = \omega_n + \Delta_n$, and $\Delta_n = \frac{-1}{\hbar\epsilon_0} \mathbf{d}_n^\dagger \cdot \text{Re} \{ \mathbf{G}(\mathbf{r}_n, \mathbf{r}_n; \omega_n) \} \cdot \mathbf{d}_n$ is the photonic Lamb shift; the dipole-dipole coupling terms are $\delta_{n,n'}|_{n \neq n'} = \frac{-1}{\hbar\epsilon_0} \mathbf{d}_n^\dagger \cdot \text{Re} \{ \mathbf{G}(\mathbf{r}_n, \mathbf{r}_{n'}; \omega'_n) \} \cdot \mathbf{d}_{n'}$ and $\Gamma_{n,n'} = \frac{2}{\hbar\epsilon_0} \mathbf{d}_n^\dagger \cdot \text{Im} \{ \mathbf{G}(\mathbf{r}_n, \mathbf{r}_{n'}; \omega'_n) \} \cdot \mathbf{d}_{n'}^1$. We have also kept the notation general to include more QDs, e.g., to include also the more usual dipole-dipole interactions between different QDs. The cw pump term $H_{\text{drive}} = \sum_n \frac{\hbar\Omega_n}{2} (\sigma_n^+ + \sigma_n^-)$ represents a possible external coherent drive applied to each dipole at laser frequency ω_L , where the effective Rabi field $\Omega_n = \langle \hat{\mathbf{E}}_{\text{pump},n}(\mathbf{r}_n) \cdot \mathbf{d}_n \rangle / \hbar$ [19]. To study the dominant radiative coupling effects we also neglect pure dephasing processes, though these can easily be included, e.g., by adding $\sum_n \gamma'_n \mathcal{L}[\sigma_n^+ \sigma_n^-]$ to Eq. (3).

In the above derivation, the Rabi fields and coupling terms (in units of frequency) are smaller than the frequency scale over which an appreciable change in the LDOS occurs, so that the scattering rates are essentially pump independent [20] and the Born and Markov ap-

¹ Note $\text{Re}[\mathbf{G}(\mathbf{r}, \mathbf{r})]$ formally diverges but we work here with the transverse Green function ($\mathbf{G} = \mathbf{G}_{\text{wg}}$, which has no divergence) and the vacuum contribution can be included by redefining the exciton transition frequencies to include this effect.

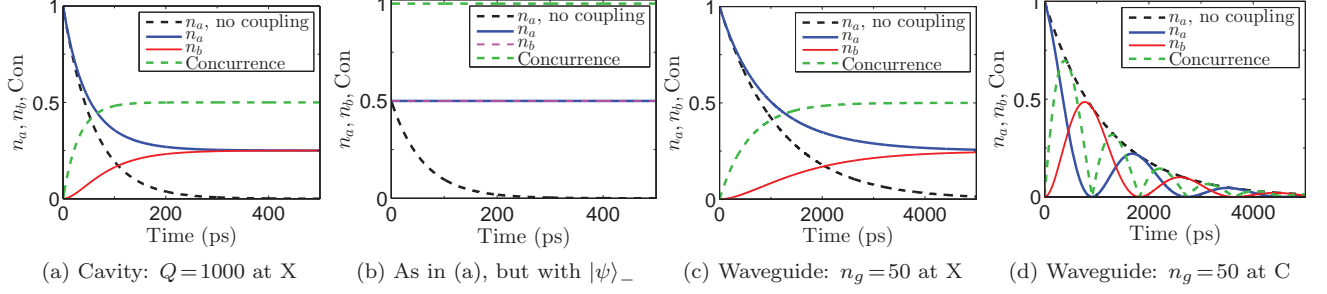


FIG. 2: Free field evolution of a QD two-dipole system with an initially excited QD population. Exciton a (blue solid) is initially excited and the AVI causes QD b (red dashed) to be excited. The entanglement of formation (concurrence) is also shown in green dashed. The population decay without the AVI is shown in black dashed.

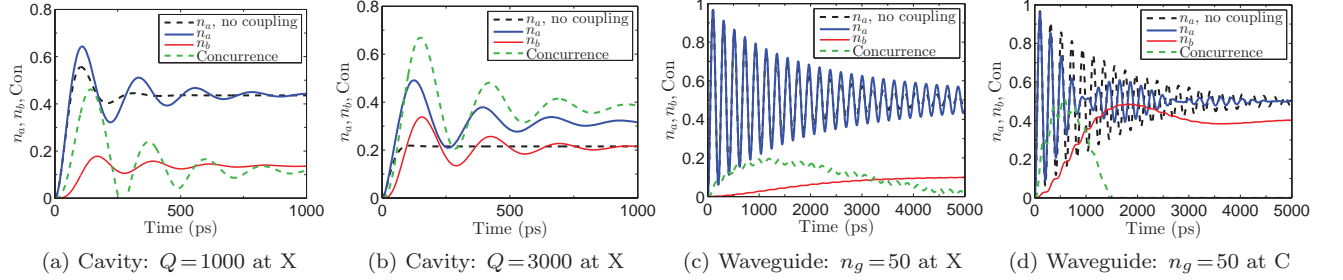


FIG. 3: Examples of a pumped QD two-dipole system. Exciton a (blue solid) is pumped with $\Omega_a = 0.02$ meV ($\approx 20\Gamma_a$ for the waveguide) cw driving field, and the AVI causes QD b (red dashed) to be excited. The concurrence is again shown in green dashed.

proximations are valid [19]. Thus, for the PC waveguide and microcavity systems considered in this work, the coupling rates are assumed to be in the weak-coupling regime. Also note that this master equation (3) is more general than the one in Ref. [1], as there are no requirements about the dipoles decaying to the same final state, and we also include coupling through the real part of the Green function, thus accounting for photon exchange through both real and virtual photons. This latter effect is particularly important at chiral points.

Let us first discuss the usual SE rate from a single dipole in a generalized medium:

$$\Gamma_a = \frac{2}{\hbar\epsilon_0} \mathbf{d}_a^\dagger \cdot \text{Im} \{ \mathbf{G}(\mathbf{r}_0, \mathbf{r}_0; \omega'_a) \} \cdot \mathbf{d}_a, \quad (4)$$

showing that the single dipole emission is proportional to the \mathbf{d}_a -projected LDOS as expected. In order to characterize the strength of the dipole-medium coupling, we introduce the enhanced SE factor or generalized Purcell factor through $F_P = \Gamma_a/\Gamma_a^0$, where Γ_a^0 is the homogeneous medium SE factor which can be obtained by using the homogeneous medium, \mathbf{G}^B , in Eq. (4). In addition, there is a possible dipole-dipole coupling term given by

$$\Gamma_{a,b} = \frac{2}{\hbar\epsilon_0} \mathbf{d}_a^\dagger \cdot \text{Im} \{ \mathbf{G}(\mathbf{r}_0, \mathbf{r}_0; \omega'_b) \} \cdot \mathbf{d}_b, \quad (5)$$

and since \mathbf{d}_a and \mathbf{d}_b are orthogonal for realistic QDs, this term is usually assumed to be negligible if \mathbf{G} is isotropic.

However, AVI effects are possible at certain locations. Below we mainly consider two coupling scenarios shown in Fig. 1, with (a) charged excitons coupled to an L point, and (b) neutral excitons coupled to a C point. In both cases, we can induce an almost perfect AVI dipole-dipole coupling, e.g., in (a): $d_a = \sigma^+$ (right circularly polarized), $d_b = \sigma^-$ (left circularly polarized) with $\mathbf{e}_k \propto E_x$, so neglecting constants and assuming $d_1 = d_2$ and that $\mathbf{G}(\mathbf{r}_0, \mathbf{r}_0)$ is complex (e.g., on-resonance for the cavity system), then $\Gamma_{a,b} = \Gamma_a = \Gamma_b$, and $\delta_{a,b} = 0$. In (b): $d_a = \sigma^x = d_b = \sigma^y$ with $\mathbf{e}_k \propto E_x + iE_y$, so $\Gamma_{a,b} = 0$, but now $\delta_{a,b} = i\Gamma_a = i\Gamma_b$; this latter scenario causes a complex frequency shift to appear in the Bloch equations, inducing different coupling dynamics to case (a).

Free-field evolution: modified vacuum dynamics. We now consider the scenario of exciton a excited, with the exciton b in the ground state. For the QD dipoles, we assume equal resonance energies at $\omega_0/2\pi = 200$ THz with dipole strength $d = 30$ D, with either $\mathbf{d}_a = d_x$ (x -polarized), $\mathbf{d}_b = d_y$ (x -polarized) or $\mathbf{d}_a = d_R$ (R -polarized), $\mathbf{d}_b = d_L$ (L -polarized). For simplicity we also neglect pure dephasing associated with charge noise, and recent experiments [21] have shown that such rates can be suppressed to less than a KHz; although our approach can include such processes, they do not affect any of our qualitative predictions that follow. For the cavity system, we use numbers typical for PC systems [15], and allow Q

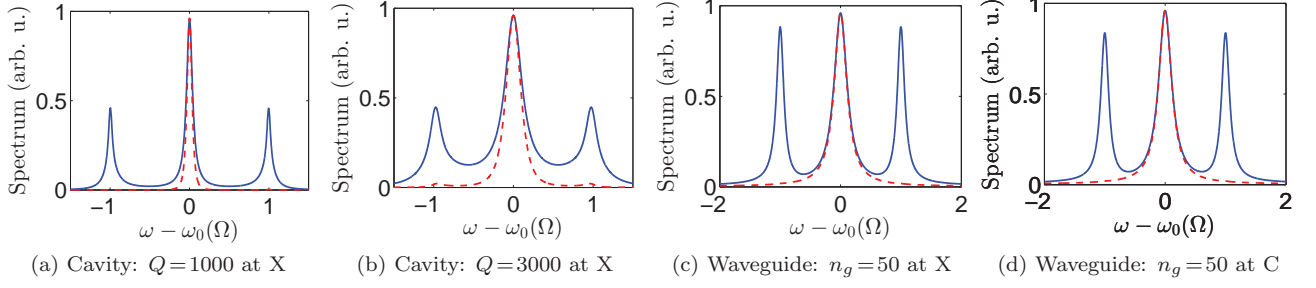


FIG. 4: Incoherent spectra (Mollow triplets) from exciton- a and exciton- b when only exciton- a is pumped. (a-b) Cavity results for different Q , when $\Omega_a = 0.012$. (c-d) Waveguide results at the X-point and C-point, respectively, with $\Omega_a = 0.004$ meV. For clarity, the frequency units are in terms of the Rabi field.

to vary, with $\varepsilon_b = 13$ and $V_{\text{eff}} = 5 \times 10^{-20} \text{ m}^3$; and for the slow-light PC waveguide, we use $V_{\text{eff}} = 4 \times 10^{-20} \text{ m}^3$, $n_g = c/v_g = 50$, $a = 400 \text{ nm}$. After solving the master equation (Eq. 3), the populations are readily computed from $n_{a/b}(t) = \langle \sigma_{a/b}^+ \sigma_{a/b}^- \rangle$.

Figure 2(a) shows the population dynamics with and without the AVI, and we also show the concurrence [22] as a measure of entanglement between the two qubits. The AVI is shown to produce a long lived entangled state, with a population transfer that is orders of magnitude larger than previously reported schemes. Note that if the initially excited state is an antisymmetric entangled pair state, $|\psi\rangle_- = \frac{1}{\sqrt{2}}[|a\rangle|0\rangle - |0\rangle|b\rangle]$, (e.g., cases (a) and (c) in Fig. 1), then there is perfect entanglement and no radiative decay at all (see Fig. 2(b)), while the symmetric initial pair state $|\psi\rangle_+ = \frac{1}{\sqrt{2}}[|a\rangle|0\rangle + |0\rangle|b\rangle]$ increases the nominal decay by a factor of exactly two (perfect super-radiance). Figures 2(c)-(d) display the waveguide results at the X-point and C-point, respectively, with the corresponding dipole polarizations; in the latter case, $\Gamma_{a,b} = 0$, but now the coupling occurs through the $\delta_{a,b}$ term which results in a complex frequency shift.

CW-pumped entanglement dynamics. Next we look at the situation where one of the QD excitons is coherently pumped, e.g., with an external laser source. Normally this would be very difficult to do with spatially coupled dots in the near-field (since both dots would be excited), but since the dipoles here are orthogonal one can selectively excite only one dipole with the appropriate pump field polarization. We consider the case where only exciton a is pumped and explore various cavity and waveguide couplings as shown in Fig. 3. First we see that the larger $Q = 3000$ cavity results in substantially more cw entanglement, compared to the $Q = 1000$ cavity of the waveguide coupling results. This reinforces the need to find systems that exhibit AVI in a large Purcell factor regime. Secondly, again we see complex interference occurs at the C-point in the PC waveguide through the complex coupling term $\delta_{a,b}$, even though $\Gamma_{a,b}$ is zero. With regards to the corresponding enhanced SE rates,

the Purcell factor in the waveguide, $F_P \approx 32$; and for the $Q = 1000$ cavity, $F_P \approx 109$ —which are quite modest and certainly achievable experimentally.

CW-pumped Mollow triplets. One of the most striking experimental signatures of high-field cw driven two-level systems is the Mollow triplet [23], which results from transitions between the field-driven dressed states. Recently the Mollow triplet in QD systems has been observed in a numbers of QD cavity systems [24–26]. Using the master equation (3) and the quantum regression theorem, the incoherent spectrum emitted from each QD exciton is obtained from [19]

$$S_0^{a/b}(\omega) = \lim_{t \rightarrow \infty} \text{Re} \left[\int_0^\infty d\tau \langle \sigma_{a/b}^+(t+\tau) \sigma_{a/b}^-(t) \rangle - \langle \sigma_{a/b}^+(t) \rangle \langle \sigma_{a/b}^-(t) \rangle e^{i(\omega_L - \omega)\tau} \right], \quad (6)$$

where we assume the detector is aligned with the corresponding polarization and we ignore additional filtering effects associated with light propagation from the QD to the detector, though these effects can be included [27]. We also consider the case where the QD excitons are directly pumped with an effective Rabi field, otherwise they will scale with Q and n_g if pumped through the cavity mode and PC waveguide mode, respectively.

Figure 4 shows the ensuing Mollow triplets from both dipoles when only dipole a is excited. In the case of a cavity, for $Q = 1000$, a Mollow triplet occurs for dipole- a , but only a singlet appears for dipole b . However, for the larger Q cavity, a spectral triplet is visible also for dipole b . For the waveguide case, we see a clear Mollow triplet for dipole a , and only a singlet with some extra spectral width at the wings for dipole b . The X-point and C-point coupling result in similar spectral features, with the X-point sidebands being slightly more pronounced.

Conclusion. We have introduced several practical QD systems that can yield substantial dipole-dipole coupling between orthogonal dipoles within the same QD, through carefully nanoengineering the photonic AVI effects. This AVI coupling can be used to coherently couple the dipoles, even though they are orthogonal, and in gen-

eral such effects may also show up in a number of emerging experiments. We have also shown that these AVI effects are quite general, occurring without the need to decay to the same final state and manifesting also through a complex Lamb shift at experimentally-accessible chiral points in PC waveguides. For an antisymmetric entangled pair state, the dipole-dipole coupling completely cancels radiative decay from the dominant cavity mode under investigation.

We thank Andrew Young and Ben Lang for useful discussions. This work was funded by the Natural Sciences and Engineering Research Council of Canada (NSERC) and Queen's University.

-
- [1] G. S. Agarwal, Phys. Rev. Lett. **84**, 5500 (2000).
 - [2] G. xiang Li, F. li Li, and S. yao Zhu, Phys. Rev. A **64**, 013819 (2001).
 - [3] P. K. Jha, X. Ni, C. Wu, Y. Wang, and X. Zhang, Phys. Rev. Lett. **115**, 025501 (2015).
 - [4] L. Sun and C. Jiang, Opt. Exp. **24**, 7719 (2016).
 - [5] S. Axelrod, M. K. Dezfouli, H. M. K. Wong, A. S. Helmy, and S. Hughes, arXiv:1606.06957 (2016).
 - [6] P. Lodahl, S. Mahmoodian, and S. Stobbe, Rev. Mod. Phys. **87**, 347 (2015).
 - [7] A. J. Brash, L. M. P. P. Martins, F. Liu, J. H. Quilter, A. J. Ramsay, M. S. Skolnick, and A. M. Fox, Phys. Rev. B **92**, 121301 (2015).
 - [8] M. A. M. Versteegh, M. E. Reimer, P. J. P. A. G. Klaus D. Jö ns, Dan Dalacu, A. Giudice, and V. Zwiller, Nature Communications **5**, 5298 (2014).
 - [9] M. Müller, S. Bounouar, K. D. Jö ns, M. Glässl, and P. Michler, Nature Photonics **8**, 224 (2014).
 - [10] R. Trotta, J. Martin-Sanchez, J. S. Wildmann, anni Piredda, Reindl, C. Schimpf, E. Zallo, S. Stroj, J. Edlinger, and A. Rastelli, Nature Communications **7**, 10375 (2016).
 - [11] S. Sun, H. Kim, G. S. Solomon, and E. Waks, Nature Nanotechnology **11**, 539 (2016).
 - [12] A. B. Young, A. C. T. Thijssen, D. M. Beggs, P. Androvitsaneas, L. Kuipers, J. G. Rarity, S. Hughes, and R. Oulton, Phys. Rev. Lett. **115**, 153901 (2015).
 - [13] I. Söllner, S. Mahmoodian, S. L. Hansen, L. Midolo, A. Javadi, G. Kiraanske, T. Pregnolato, H. El-Ella, E. H. Lee, J. D. Song, S. Stobbe, and P. Lodahl, Nature Nanotechnology **10**, 775 (2015).
 - [14] V. S. C. Manga Rao and S. Hughes, Phys. Rev. B **75**, 205437 (2007).
 - [15] P. Yao, V. S. C. Manga Rao, and S. Hughes, Laser Photon. Rev. **4**, 499 (2009).
 - [16] G. S. Agarwal, Phys. Rev. A **12**, 1475 (1975).
 - [17] H. T. Dung, L. Knöll, and D.-G. Welsch, Phys. Rev. A **66**, 063810 (2002).
 - [18] G. Angelatos and S. Hughes, Phys. Rev. A **91**, 051803 (2015).
 - [19] H. Carmichael, *Statistical Methods in Quantum Optics 1: Master Equations* (Springer, 1999).
 - [20] R.-C. Ge, C. Van Vlack, P. Yao, J. F. Young, and S. Hughes, Phys. Rev. B **87**, 205425 (2013).
 - [21] N. Somaschi, V. Giesz, L. D. Santis, J. C. Lored, M. P. Almeida, G. Hornecker, S. L. Portalupi, T. Grange, C. Anton, J. Demory, C. Gomez, I. Sagnes, N. D. Lanzillotti-Kimura, A. Lemaitre, A. Aufferes, A. G. White, L. Lanco, and P. Senellart, Nat. Photon. **10**, 34 (2016).
 - [22] W. K. Wootters, Phys. Rev. Lett. **80**, 2245 (1998).
 - [23] B. R. Mollow, Phys. Rev. **188**, 1969 (1969).
 - [24] E. B. Flagg, A. Muller, J. W. Robertson, S. Fountal, D. G. Deppe, M. Xiao, W. Ma, G. J. Salamo, and K. Shih, Nature Physics **5**, 203 (2009).
 - [25] A. N. Vamivakas, Y. Zhao, C.-Y. Lu, and M. Atatüre, Nature Physics **5**, 198 (2009).
 - [26] S. Ates, S. M. Ulrich, S. Reitzenstein, A. Löffler, A. Forchel, and P. Michler, Phys. Rev. Lett. **103**, 167402 (2009).
 - [27] F. Hargart, M. Müller, K. Roy-Choudhury, S. L. Portalupi, C. Schneider, S. Höfling, M. Kamp, S. Hughes, and P. Michler, Phys. Rev. B **93**, 115308 (2016).